Metals & corrosion

Pore tracing in additive manufactured and hot isostatic pressed components

Natan Nudelis[1,2,*] , and Peter Mayr[1]

[1] *TUM School of Engineering and Design, Chair of Materials Engineering of Additive Manufacturing, Technical University of Munich, Munich, Germany*
[2] *FIT AG, Lupburg, Germany*

ABSTRACT

Despite past scientific efforts and the increased use of hot isostatic pressing (HIP) in additive manufacturing applications, a complete understanding of the exact pore-closing behaviour has yet to be achieved. The present research focuses on laser powder bed fused (LPBF), hot isostatic pressed components made of AlSi10Mg, and process-related defects. The study shows the effect of HIPing in relation to various pore characteristics, such as pore shape, size, and type. A pore tracing method using X-ray data was developed to characterise the pores before and after HIP. The method is based on the k-nearest neighbours approach and allows to match leftover pores with the initial ones. Hence, the efficiency of the pore-closing behaviour for different HIP settings can be analysed. Moreover, the exact number of pore transformations can be tracked, providing a comprehensive insight into the change of pore characteristics during HIP. In this framework, eight different HIP settings and a total number of 274,886 pores were examined and discussed. The findings demonstrate that longer treatment times and higher pressure and temperature settings accelerated the pore transformation. Irregularly shaped and large pores close faster than spherically shaped and smaller ones. Furthermore, regardless of the initial pore type, all pores started transforming their shape towards irregular shapes and small pore diameters. Some pores remained after the HIP treatments, probably due to the inefficiency of HIP in closing pores connected with the component surface or the presence of oxide particles interfering with the diffusion bonding process.

Introduction

Hot isostatic pressing (HIP) is a densification process under high pressure at elevated temperatures, typically used to densify powders, casts or sintered components made of metals or ceramics. The gas pressure in the press acts uniformly in all directions, resulting in isotropic component properties. Nowadays, hot isostatic pressing of additively manufactured components is acknowledged for its ability to generate

---

Handling Editor: Sophie Primig.

Address correspondence to E-mail: natan.nudelis@pro-fit.de

🙋 Springer

parts of high relative density and with a homogeneous microstructure [1–6]. Post-processing, including HIP, is a critical phase in the AM workflow as it helps to achieve the desired mechanical properties, geometric accuracy, and surface finish. A very thorough review of post-processing in additively manufactured metallic components can be found in Malakizadi et al. [7]. X-ray tomography was already recognised as an appropriate tool to provide insights into pore-closing behaviour [1, 3, 6]. Despite past scientific efforts, the yield from X-ray data has yet to be fully exploited. The knowledge about the exact transformation behaviour of each detected pore before and after HIP can expand the existing understanding and lead to optimised HIP cycles.

In literature, three pore types are most frequently mentioned in AlSi10Mg components made by laser powder bed fusion (LPBF). Hydrogen-induced, keyhole-, and lack-of-fusion pores can be distinguished by their shape, size, and cause of origin. Hydrogen-induced pores are spherically shaped, less than 100 μm in diameter and preferably formed at slow laser scanning speeds [8]. The nucleation and growth of hydrogen-induced pores depend highly on the local hydrogen content and the solubility in solid and liquid aluminium, which differs by factor 10. Due to these facts, the trapped hydrogen will enrich at the solidification front of the melt pool if the hydrogen content is higher than the solubility limit in the solid phase [9]. Moreover, keyhole pores occur when the melting mechanism changes to "keyhole-mode" laser beam melting, which is controlled by the evaporation of metal due to the high-power density of the laser beam [10]. The collapse of capillary cavities finally leads to the formation of pores in the root of the melt pool. These pores are spherically shaped, large in diameter and filled with trapped gas from the process chamber. Furthermore, lack-of-fusion pores occur due to insufficient laser energy input into the powder bed. On the one hand, lack of fusion can be caused by weld spatter agglomerations, which are many times larger in volume and diameter (between 200 and 500 μm) than the average powder particle [11]. Those weld spatter agglomerations would need far more laser energy to be entirely melted, which is not provided by the process. On the other hand, lack of fusion can be caused by oxide particles, which appear due to an oxidation process on the scanned layers or at the boundaries of the melt pool [12]. All lack-of-fusion pores have in common that they are irregularly shaped and large in

diameter, partially filled with unmolten powder particles. Additionally, the formation of pores is dependent on the process conditions, applied process parameters, and scanning strategies. Read et al. [13] noted that laser power, scanning speed, and their interplay significantly affect porosity. Hasmuni et al. [14] observed that the hatch distance, which controls the overlap amongst the scan tracks, also impacts the formation of pores. Especially, lack-of-fusion pores occur due to insufficient laser energy input into the powder bed, which is caused by several process-related influences.

This study introduces a novel pore tracing method using X-ray data to rigorously explore the pore transformations during different HIP treatments. The subsequent sections delve into the methodology and findings that underpin this exploration.

Methods

Details of the manufacturing, post-processing, and scanning process

For the X-ray scans, cylindrical specimens with a diameter of 10 mm and a height of 18 mm were used. The analysed specimens were fabricated at FIT AG using an LPBF machine SLM500 (SLM Solutions, Lübeck, Germany), which is equipped with an Nd:YAG-laser (λ = 1064 nm). The used material was AlSi10Mg (Tekna Advanced Materials Inc., Sherbrooke, Canada) with a chemical composition of 9.5 weight % Si, 0.29 weight % Mg, 0.09 weight % Fe, 0.03 weight % Ti, and 0.032 weight % O. Elements such as Cu, Mn, Ni, Zn, Pb, Sn, N, and H were ≤ 0.005 weight %. All cylindrical specimens were produced with a laser power of 350 W, a laser scanning speed of 1,150 mm/s, a layer thickness of 50 μm, and a hatch spacing of 0.17 mm. The spot size diameter of the laser beam was set at 0.08 mm. The building direction was fixed vertically to the building platform. All specimens were built using a strip scanning strategy with an 83 degree rotation at each layer. Furthermore, the contour of each specimen consists of two laser lines. The SLM500 chamber was filled with nitrogen gas of purity 99.999 %. Within the scope of this work, eight different HIP cycles using a Quintus 32 1400 M URQ (Västerås, Sweden) were carried out. The samples were treated at 480 °C or 540 °C, under high pressure of 300 or 2000 bar, and a holding time of 30 or 90 min. The furnace was filled with argon gas of purity 99.999 %. A total of 274,886 pores were

examined in eight specimens detected by X-ray scans. The X-ray scans were made using a Diondo d2 microfocus CT system (Hattingen, Germany) with a minimum voxel size of 9.659 μm^3. Each scan was carried out in 1500 projections in a 360° sample rotation (1.4 s integration time per projection) using a power output of 9.5 W and a voltage of 190 kV. The reconstruction of raw CT data into a 3D model was performed with VGSTUDIO MAX 3.1.0 64 (Volume Graphics, Heidelberg, Germany). The analysed region of interest (ROI) includes a volume of 785.4 mm^3. The porosity within the ROI was analysed using the VGDefx algorithm (Volume Graphics, Heidelberg, Germany).

Pore classification method using computed tomography data

Nowadays, the fundamentals of the formation of pores in laser powder bed fusion are already well understood. Besides local inconsistencies, these pores can also be seen as an individual process fingerprint containing comprehensive information on the process conditions. Moreover, already existing pore classification methods help to exploit this individual information. The utilised classification method is taken from the authors' previous work [15]. It classifies the pore shape into spherical and irregular shapes using three shape indicators (Ψ, Ω and *BB-factor*). The sphericity is expressed as the ratio of the surface area of a sphere (with the same volume as the given pore) to the pore's surface area. The compactness is defined as the ratio of the pore volume to the volume of a sphere, represented by the maximum diameter surrounding the pore. The BB-factor is described as the ratio between the smallest and the largest dimensions of the bounding box. All classification criteria are shown in Table 1. The pores are divided into six classes (A–F), where class A–C describe spherically shaped pores and D–F irregularly shaped pores. Combined with the information about the pore size (maximum diameter around

the pore), classifying pore types such as hydrogen-induced, keyhole, and lack-of-fusion pores are possible. Additional descriptions of the pore classification method can be found in [15].

Pore tracing method using computed tomography data

The following pore tracing method using X-ray data was developed to retrieve pores in additive manufactured samples before and after HIPing. Figure 1 illustrates the methodical approach of pore matching. Accordingly, a cylindrical sample must be CT-scanned twice, once directly after the manufacturing process and a second time after HIPing. This creates pore clouds, which include three-dimensional information about the exact pore location. It is important to emphasise that the samples must be CT-scanned as precisely as possible and in the same orientation. Furthermore, a point cloud registration using the iterative closest point (IPC)-algorithm was carried out to lay over the leftover pores after HIPing with the initial existing ones. Using the k-nearest neighbour method, the pores with the highest match probability can be found. Figure 1 shows an example of pore matching. The k-nearest neighbour algorithm randomly chooses a leftover pore after HIPing and calculates k-spheres around the leftover pore. Each sphere represents the Euclidian distance from the HIPed pore to the initial ones. A pore match is recognised for the closest Euclidian distance between the HIPed pore and the initial pore (k = 1). The identified pore match will be removed from the pore cloud, and the procedure will be repeated with another leftover pore until no more leftover pores exist. The code, including all named tools, was created using MATLAB R2021b (MathWorks, Natick, USA).

Table 1 Pore classification criteria using X-ray data [15]

| Pore class		Diameter	Compactness	Sphericity	BB-factor
Spherical	A	$D_{pore} \leq 100\ \mu m$	$\Omega \geq 0.4$	$\Psi \geq 0.6$	$BBF \geq 0.6$
	B	$100\ \mu m < D_{pore} \leq 200\ \mu m$			
	C	$D_{pore} > 200\ \mu m$			
Irregular-shaped	D	$D_{pore} \leq 100\ \mu m$	$\Omega < 0.4$	$\Psi < 0.6$	$BBF = [0,1]$
	E	$100\ \mu m < D_{pore} \leq 200\ \mu m$			
	F	$D_{pore} > 200\ \mu m$			
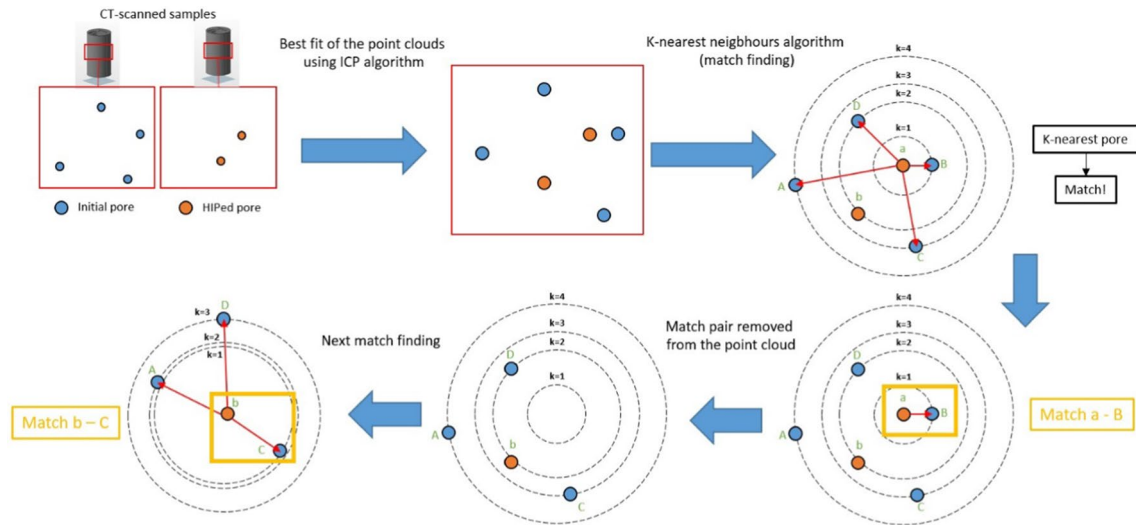
Figure 1 Methodical approach of pore matching.

Results and discussion

The pore tracing method provides a comprehensive insight into the pore transformation behaviour during hot isostatic pressing. The pore-closing behaviour, which can be analysed for different HIP parameters, depends on various pore characteristics, such as pore shape, size, and type. On this account, all pores were categorised into six classes (A–F) according to the presented classification method. A typical pore classification result of a cylindrical sample made by laser powder bed fusion under defined process conditions is exemplified in Fig. 2. The figure shows a total number of 33,305 pores depending on their compactness and diameter. In this example, irregularly shaped pores appear to originate more often (class D: 49.48 %, class E: 17.98 %, class F: 0.59 %) than spherically shaped pores (class A: 25.39 %, class B: 6.55 %, class C: 0.01 %).

Eight different HIP process parameter settings were analysed using the pore classification [15]—and pore tracing method to foster an increased understanding of the HIP process. Figure 3 illustrates the leftover pores after HIPing for each parameter set. The findings demonstrate that longer treatment times, higher pressure, and temperature improve pore-closing results. Li et al. [16] observed a 96 % reduction in pore volume after the first HIP step of increasing temperature and pressure. Moreover, Prasad et al. [17] showed an effective porosity reduction by increasing the applied pressure or the holding time. Almost all leftover pores are irregularly shaped and small in size. Regardless of the set HIP parameters, the pores change from spherical to irregular shapes and from larger to smaller diameters. Irregularly shaped pores will most likely dictate component failure, most often by the propagation of a single dominating crack. Therefore, an uncompleted pore-closing procedure should be avoided. Some pores remained, even after long treatment times and

Figure 2 Pore classification result of a cylindrical sample made by laser powder bed fusion.
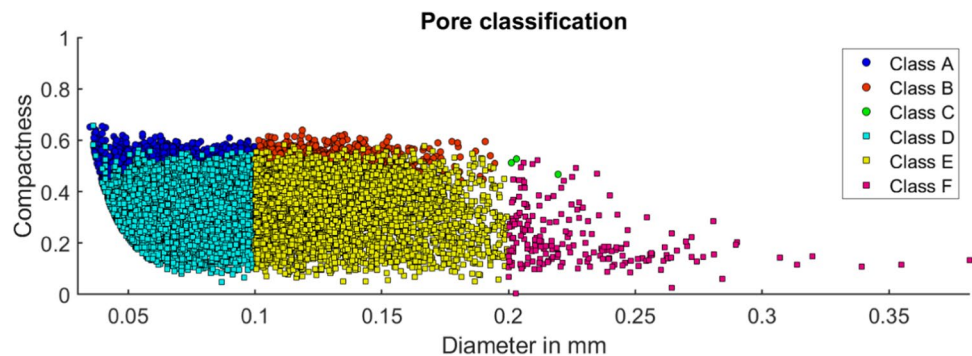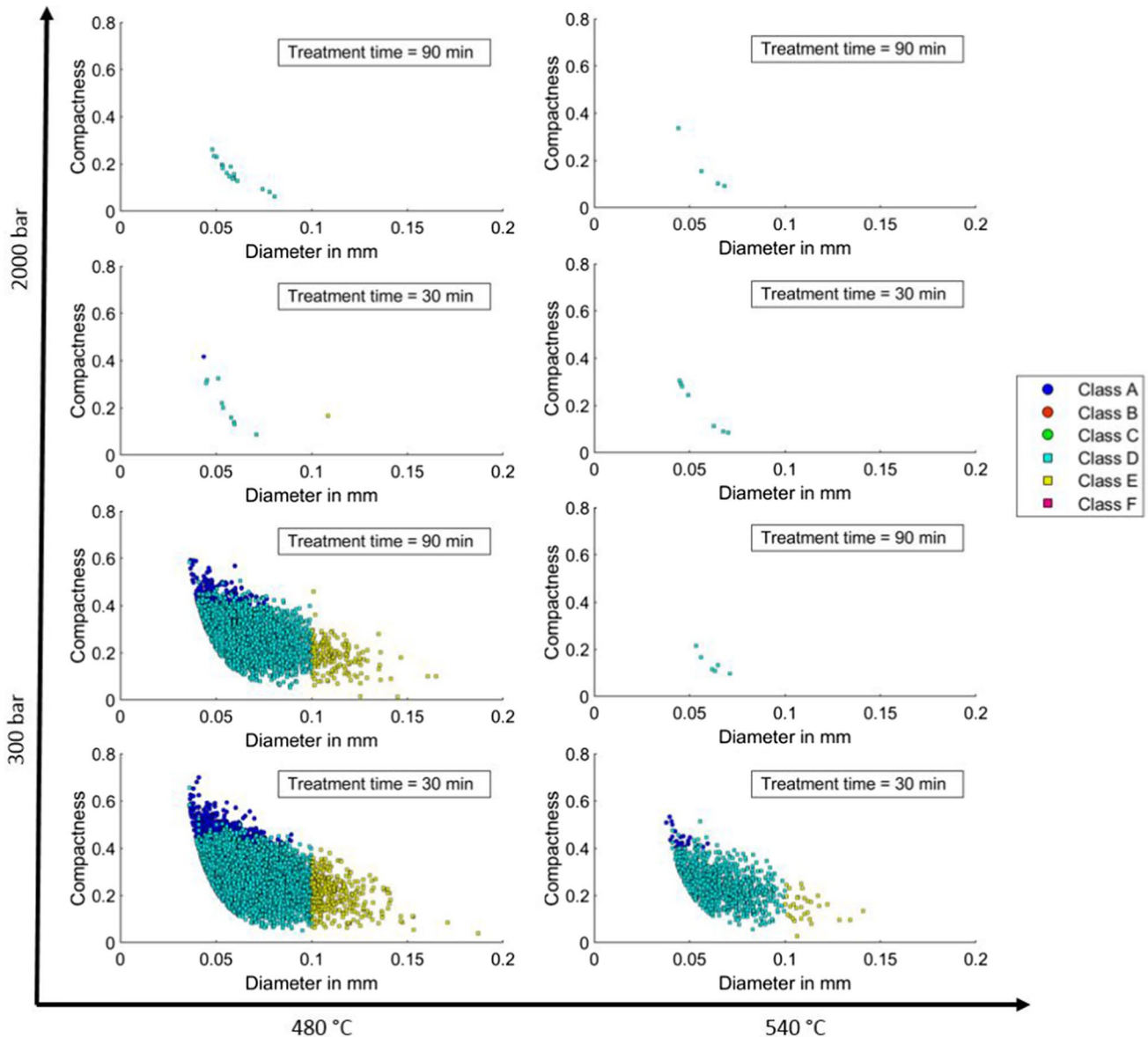
Figure 3 Pore classification results after eight different HIP treatments.

high temperature and pressure settings. This can be explained by the inefficiency of HIPing to close pores at or connected to the component surface [18]. The argon gas has no consolidation force acting on the pore if the defect has a connection to the surface [3]. Only closed voids can be identified as pores in the X-ray scans, as the software (Volume Graphics) cannot differentiate between the part surface and a surface defect. The leftover pores after HIPing indicate that a connection to the surface existed below the resolution of the X-ray scan. Although almost all initial pores could be compressed during some HIP treatments, this does not necessarily mean they are diffusion bonded. A subsequent heat treatment or stress concentration could reopen the pore [19]. The main densification mechanisms during HIP treatment are plastic yielding, power law creep, Nabarro-Herring, and Coble creep or diffusion [20]. Coble [21] assumed that an applied compressive stress would reduce the concentration of vacancies at grain boundaries. This would promote the diffusional movement of material towards the voids, aiding in the closure of the pores. The reason for insufficient fusion (e.g. diffusion bonding) of the pores can be caused by oxide particles. Oxide particles appear

due to an oxidation process on scanned layers and at the boundaries of the melt pool [12]. Moreover, Tang et al. [22] observed oxide particles most often at pore interfaces. Hence, it is assumed that diffusion bonding in AlSi10Mg components did not fully progress due to the presence of oxides [1].

To explain the exact transformation of pores during hot isostatic pressing, a closer look at the pore tracing results has to be made. Figure 4 shows the pore tracing results for one of the presented HIP cycles (480 °C, 300 bar, 30 min). All pores found by pore matching, which were not completely closed during the HIP treatment, are illustrated. The same pores before and after HIPing and the exact number of pore-type transformations are shown. The dominating change of each pore class to another is shown using arrows. All pores started transforming their shape towards irregular shapes and smaller pore diameters. Regardless of the initial size of the pore, all irregularly shaped pores (class D–F) transformed to the small and irregularly shaped class D. This proves that larger pores close faster than smaller ones. Furthermore, it seems that spherically shaped pores need more time to be eliminated than irregularly shaped ones. For instance, class C (large and spherical pores) transformed partly to a medium size diameter (class E) instead of a small size (class D). During a HIP cycle, the high isostatic pressure increases stress concentrations at pore sites,

which drives the pore-closing process. Nudelis et al. [15] used an FEA analysis and determined that large and irregularly shaped pores tend to have the highest stress concentrations during load. On the other hand, spherical pores do not have any cross-sectional transitions, which can cause such high-stress concentrations. Irregularly shaped pores close faster than spherical ones because of higher stress concentrations. Budiansky et al. [23] assumed that small deviations from the hydrostatic stress cause spherical pores to collapse into penny-shaped or rod-shaped pores. These deviations can occur during HIP due to the interaction of the stress state around neighbouring pores, resulting in a process of pore shape change instability [18]. It is important to emphasise that regardless of the HIP parameter settings, the exact behaviour of pore-closing occurred. The increase in pressure, time, and temperature only accelerated the pore transformation.

A reliability check of the method must be done to assess the tracing results. Using two identical pore clouds allow us to test the method. The resulting class transformations and the number of failed match formations are reliability indicators. The success of the tracing method primarily depends on the total amount of possible pore matches and the displacement of the two pore clouds relative to each other. The HIPed pore cloud in Fig. 4 was used for the reliability check. In this case, 12,419 pores remained after HIP in the pore
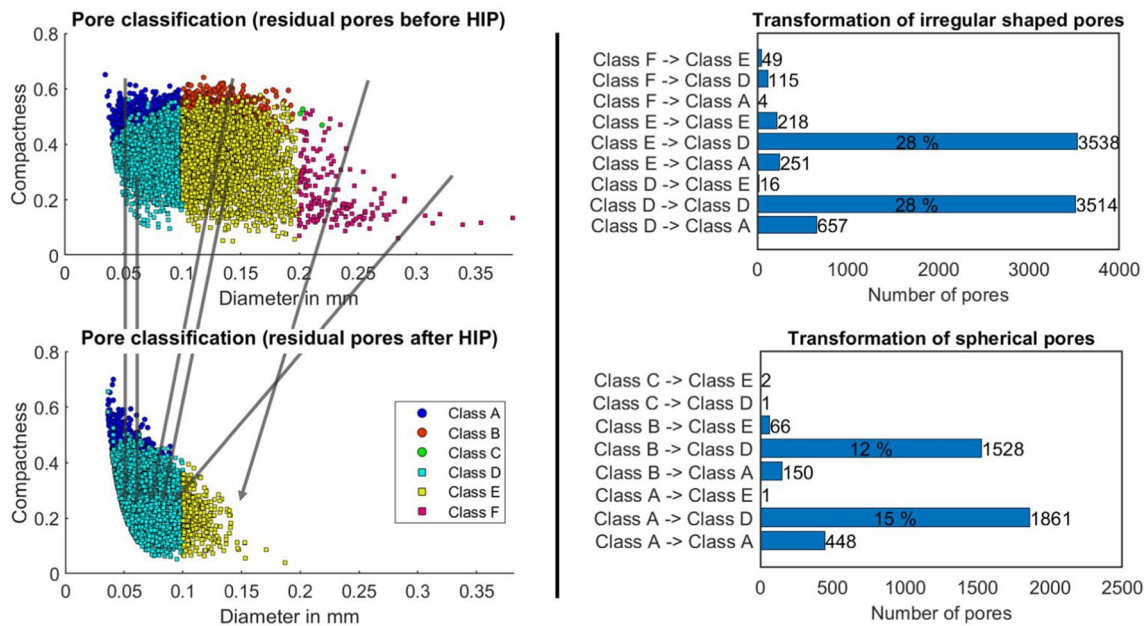

Figure 4 Pore tracing result of a representative HIP cycle (480 °C, 300 bar, 30 min).

classes A, D, and E. These leftover pores were matched to the initial ones. Without any artificial displacements of the two identical pore clouds, the number of failed pore match formations is 1. All pore matches remained in the same pore class (number of misclassification = 0). In other words, if the CT scans were carried out in the same orientation without any displacements, the total error would be 0.008 %. Moreover, the errors with a displacement in the z-direction were tested. If a z-displacement of 50 μm is applied, the absolute error is 0.153 % (no match = 1; number of misclassifications = 18). The error increases with increasing pore cloud displacements. A z-displacement of 100 μm caused an error of 7.633 % (no match = 50; number of misclassifications = 898). In conclusion, samples before and after HIPing must be CT-scanned as precisely as possible and in the same orientation. The lower the pore cloud shift, the more reliable the result. It is important to emphasise that each pore cloud pair is individual and can have different error values. A movement of pores during HIPing is also a possible scenario. Within the framework of this work, the scans were scanned as accurately as possible.

Summary and conclusions

In fostering an increased understanding of the HIP process, a novel pore tracing method using X-ray data was developed. In total, eight different HIP process parameter settings were analysed using the pore classification [15]—and pore tracing approach. The findings clearly demonstrate that longer treatment times and higher pressure and temperature lead to a more successful pore-closing result. Regardless of the initial size and shape of the pore, all pores started to transform their shape towards irregular shapes and smaller pore diameters. For instance, all irregularly shaped pores (class D–F) transformed to class D with smaller sizes and irregular shapes. That proves that larger pores are closed faster than smaller ones. Furthermore, spherically shaped pores need more time to be closed completely than irregularly shaped ones. Because of higher stress concentrations, irregularly shaped pores close faster than spherical ones [15]. It is important to emphasise that irregularly shaped pores will dictate component failure, most often by the propagation of a single dominating crack. Therefore, an uncompleted pore-closing procedure should

be avoided. Some pores remained after the HIP treatments, possibly due to the inefficiency of HIP to close pores connected to the component surface, or the presence of oxide particles preventing proper diffusion bonding. Oxide particles, which arise due to oxidation processes on scanned layers and melt pool boundaries [12], can inhibit proper fusion of the pores. Regardless of the HIP parameter settings, the exact behaviour of pore-closing occurred. The increase in pressure, time, and temperature only accelerated the pore transformation. The presented pore tracing method can be used to analyse the effect of hot isostatic pressing on the pore-closing behaviour. It must be noted that displacements or inaccuracies in CT scans can introduce significant errors, underscoring the importance of their accuracy and precision. Further research should include finite element simulations to confirm the presented pore-closing results. Unresolved issues such as the interaction of the stress state around neighbouring pores or the influence of oxide particles could be clarified using finite element simulations. Moreover, the pore tracing method can serve as a data source for supervised learning methods, allowing neural networks to be trained to optimise HIP parameters for desired part quality.

Author contribution

N. N. was involved in conceptualization, methodology, data collection, data curation, formal analysis, visualisation, investigation, validation, writing—original draft, writing—review and editing. The first draft of the manuscript was written by N. N. and all authors commented on previous versions of the manuscript. All authors read and approved the final manuscript. P. M. helped in supervision, conceptualization and writing—review and editing.

Funding

Data availability

Data are available on request.

Declarations

Conflict of interest The authors declare no conflict of interest.

Code availability Code is available on request.

Ethical approval Not applicable.

Consent to participate Not applicable.

Consent for publication Not applicable.

References

[1] Hirata T, Kimura T, Nakamoto T (2020) Effects of hot isostatic pressing and internal porosity on the performance of selective laser melted AlSi10Mg alloys. Mater Sci Eng A 772:138713. https://doi.org/10.1016/j.msea.2019.138713

[2] Finfrock CB, Exil A, Caroll JD, Deibler L (2018) Effect of hot isostatic pressing and powder feedstock on porosity, microstructure and mechanical properties of selective laser melted AlSi10Mg. Metallogr Microstruct Anal 7:443–456. https://doi.org/10.1007/s13632-018-0456-z

[3] du Plessis A, Macdonald E (2020) Hot isostatic pressing in metal additive manufacturing: X-ray tomography reveals details of pore closure. Addit Manuf 34:101191. https://doi.org/10.1016/j.addma.2020.101191

[4] Wang Y, Shi J (2020) Effect of hot isostatic pressing on nanoparticles reinforced AlSi10Mg produced by selective laser melting. Mater Sci Eng A 788:139570. https://doi.org/10.1016/j.msea.2020.139570

[5] Girelli L, Giovagnoli M, Tocci M, Pola A, Fortini A, Merlin M, la Veccia GM (2019) Evaluation of the impact behaviour of AlSi10Mg alloy produced using laser additive manufacturing. Mater Sci Eng A 748:38–51. https://doi.org/10.1016/j.msea.2019.01.078

[6] Tammas-Williams S, Withers PJ, Todd I, Prangnell PB (2016) The effectiveness of hot isostatic pressing for closing porosity in titanium parts manufactured by selective electron beam melting. Metall Mater Trans A 47:1939–1946. https://doi.org/10.1007/s11661-016-3429-3

[7] Malakizadi A, Mallipeddi D, Dadbakhsh S, M'Saoubi R, Krajnik P (2022) Post-processing of additively manufactured metallic alloys—a review. Int J Mach Tools Manuf 179:103908. https://doi.org/10.1016/j.ijmachtools.2022.103908

[8] Aboulkhair NT, Everitt NM, Ashcroft I, Tuck C (2014) Reducing porosity in AlSi10Mg parts processed by selective laser melting. Addit Manuf 1–4:77–86. https://doi.org/10.1016/j.addma.2014.08.001

[9] Weingarten C, Buchbinder D, Pirch N, Meiners W, Wissenbach K, Poprawe R (2015) Formation and reduction of hydrogen porosity during selective laser melting of AlSi10Mg. J Mater Process Technol 221:112–120. https://doi.org/10.1016/j.jmatprotec.2015.02.013

[10] King WE, Barth HD, Castillo VM, Gallegos GF, Gibbs JW, Hahn DE, Kamath C, Rubenchik AM (2014) Observation of keyhole-mode laser melting in laser powder-bed fusion additive manufacturing. J Mater Process Technol 214(12):2915–2925. https://doi.org/10.1016/j.jmatprotec.2014.06.005

[11] Haeckel F, Meixlsperger M, Burkert T (2017) Technological challenges for automotive series production in laser beam melting. Proceedings of the 28th annual international Solid Freeform Fabrication Symposium. Austin, ATX, Texas. https://doi.org/10.26153/tsw/16985

[12] Louvis E, Fox P, Sutcliffe CJ (2011) Selective laser melting of aluminium components. J Mater Process Technol 211(2):275–284. https://doi.org/10.1016/j.jmatprotec.2010.09.019

[13] Read N, Wang W, Essa K, Attallah MM (2015) Selective laser melting of AlSi10Mg alloy: process optimisation and mechanical properties development. Mater Des 65:417–424. https://doi.org/10.1016/j.matdes.2014.09.044

[14] Hasmuni N, Ibrahim M, Raus AA, Wahab MS, Kamarudin K (2018) Porosity effects of AlSi10mg parts produced by selective laser melting. J Eng Mech 5(4):246–255

[15] Nudelis N, Mayr P (2021) A novel classification method for pores in laser powder bed fusion. Metals 11(12):1912. https://doi.org/10.3390/met11121912

[16] Li W, Xu Q, Yin Y, Zhou J, Nan H (2023) Research on pore closure behavior and microstructure evolution during hot isostatic pressing of Ti6Al4V alloy casting. J Mater Res Technol 24:3628–3642. https://doi.org/10.1016/j.jmrt.2023.04.027

[17] Prasad MRG, Gao S, Vajragupta N, Hartmaier A (2020) Influence of trapped gas on pore healing under hot isostatic pressing in nickel-base superalloys. Crystals 10(2):1147. https://doi.org/10.3390/cryst10121147

[18] Kellett BJ, Lange FF (1988) Experiments on pore closure during hot isostatic pressing and forging. J Am Ceram Soc 71(1):7–12

[19] Hastie JC, Kartal ME, Carter LN, Attallah MM, Mulvihill DM (2020) Classifying shape of internal pores within AlSi10Mg alloy manufactured by laser powder bed fusion using 3D X-ray micro computed tomography: influence of processing parameters and heat treatment. Mater Charact 163:110225. https://doi.org/10.1016/j.matchar.2020.110225

[20] Radomir I, Geamăn V, Stoicănescu M (2012) Densification mechanisms made during creep techniques applied to the hot isostatic pressing. Procedia Soc Behav Sci 62:779–782. https://doi.org/10.1016/j.sbspro.2012.09.131

[21] Coble RL (1970) Diffusion models for hot pressing with surface energy and pressure effects as driving forces. J Appl Phys 41:4798–4807. https://doi.org/10.1063/1.1658543

[22] Tang M, Pistorius PC (2017) Oxides, porosity and fatigue performance of AlSi10Mg parts produced by selective laser melting. Int J Fatigue 94(2):192–201. https://doi.org/10.1016/j.ijfatigue.2016.06.002

[23] Budiansky B, Hutchinson JW, Slusky S (1982) Void growth and collapse in viscous solids. Mech Solids 60:13–45. https://doi.org/10.1016/B978-0-08-025443-2.50009-4